RSC Advances

ROYAL SOCIETY OF CHEMISTRY

www.rsc.org/advances

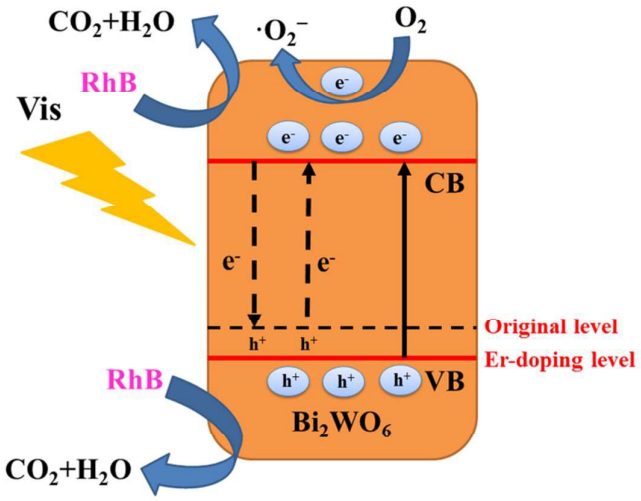

1.5% $Bi_2WO_6:Er^{3+}$ exhibited highest photocatalytic activity as the separation efficiency of the photogenerated electron–hole pairs is enhanced.

RSC Advances

PAPER

Synthesis of Er-doped Bi_2WO_6 and enhancement in photocatalytic activity induced by visible light

Received 00th January 20xx,
Accepted 00th January 20xx

DOI: 10.1039/x0xx00000x

www.rsc.org/

Meng Wang, Ziyu Qiao, MinghaoFang*, Zhaohui Huang*, Yan'gai Liu, Xiaowen Wu, Chao tang, Hao Tang, Hekai Zhu

Bi_2WO_6:Er^{3+} with hierarchical flower-like microstructures were synthesized by a one-step hydrothermal method. The photocatalysts thus obtained were characterized in detail by X-ray diffraction (XRD), scanning electron microscopy (SEM), UV–vis diffuse reflectance spectroscopy (UV–vis DRS), X-ray photoelectron spectroscopy (XPS) as well as photoluminescence (PL) measurements. Results obtained by XPS confirmed the presence of Er^{3+} dopants in Bi_2WO_6. Moreover, the results obtained from SEM have shown that doping with Er ions results in hierarchical flower-like microstructures of Bi_2WO_6. Under visible light irradiation, with an appropriate doping content, the photocatalysts exhibit significant improvement in the photocatalytic activity as the separation efficiency of the photogenerated electron–hole pairs is enhanced. Notably, the photocatalytic activity of 1.5% Bi_2WO_6:Er^{3+} is 3.69 times that of undoped Bi_2WO_6. The results indicate that an appropriate doping content can improve photocatalytic activity, caused by wider band gap, hierarchical flower-like microstructures, and defects generated by doping with Er^{3+}, which in turn increase the separation efficiency of the photogenerated electron–hole pairs.

Introduction

As the economic status of society and quality of life are improving, the issue of environmental pollution is getting worse. As a result, people are now realizing the importance of environmental governance. Currently, photocatalytic degradation has been attracting widespread attention, caused by its merits of environment friendliness, low reaction temperature, good stability, as well as use of solar energy.[1-5] Moreover, recently, visible-light-driven photocatalysts have been gaining increasing focus. As compared to traditional wide band-gap photocatalysts such as TiO_2 [6-9], bismuth tungstate (Bi_2WO_6) has a relatively narrow band gap (2.6–2.8 eV), which allows for strong absorption in the visible region of sunlight ($\lambda > 420$ nm). Thus, Bi_2WO_6 photocatalysts efficiently utilize solar energy.[10-14]

Bi_2WO_6 is the simplest member of the layered Aurivillius oxide; its crystal structure consists of alternating layers of bismuth oxide $(Bi_2O_2)^{2+}$ and $(WO_4)^{2-}$ octahedrons; furthermore, $(WO_4)^{2-}$ layers are composed of $(WO_4)^{2-}$ octahedron vertices linked together[15], resulting in outstanding photocatalytic activity for the degradation of dyes under visible light.[16] Bi_2WO_6 exhibits intense absorption and photostability under visible light; however, the life of the photogenerated electron–hole pairs is very short, and facile recombination can occur, resulting in low quantum efficiency.[17-19]

For improving the photocatalytic activity of Bi_2WO_6, doping metal or non-metal elements into Bi_2WO_6 is an efficient method for decreasing the recombination rate of the photogenerated electron–hole pairs and enhancing the visible light absorption.[20-25] Thus far, the doping of metal and non-metal elements such as Fe[26], Ag[27], and F[28] into Bi_2WO_6 has already been reported to improve the photocatalytic activity for the degradation of some dyes under visible light. In recent years, the replacement of Bi^{3+} by rare-earth ions such as Y^{3+} [29] and Gd^{3+} [30] has been reported to improve the photocatalytic activity of Bi_2WO_6. Notably, Y^{3+} and Gd^{3+} are not luminous active ions, but Er^{3+} is a type of a luminous active ion. Very few studies have focused on the modification of Bi_2WO_6 by doping with luminous active ions. Under the circumstances, the improvement is reached by increasing the number of incoming radiation photons absorbed by the photocatalyst. The luminous active ions could handle and transform the not absorbed photons into appropriate energy ones.

Er was selected because the electronic structure and light absorption of Er^{3+} are very different from those of Bi^{3+}; besides, the ionic radius of Er^{3+} (89 pm) is smaller than that of Bi^{3+} (103 pm), and the lattice parameters of Bi_2WO_6 may decrease after the substitution of for Bi^{3+} with Er^{3+}, thereby resulting in a reduced lattice spacing d. This reduction will significantly affect the optical and surface properties. To the best of our knowledge, a recent paper has explored a TiO2/Bi2WO6-Er with plate-like structure, obtain a conclusion the higher band-gap values in lower Er doped systems would be the cause of a better electron hole separation under UV irradiation.[31] In this paper, Er^{3+}-doped Bi_2WO_6 photocatalysts were synthesized by a one-step hydrothermal method. The samples showing flower-like hierarchical organization

Beijing Key Laboratory of Materials Utilization of Nonmetallic Minerals and Solid Wastes, National Laboratory of Mineral Materials, School of Materials Science and Technology, China University of Geosciences, Beijing, 100083
E-mail: fmh@cugb.edu.cn (Minghao Fang); huang118@cugb.edu.cn (Zhaohui Huang). Tel: +861082322186
† Electronic Supplementary Information (ESI) available.

and were tested under visible irradiation (λ > 420 nm). To investigate the effects and mechanism of Er^{3+} in Bi_2WO_6, the photocatalysts were characterized by X-ray diffraction (XRD), scanning electron microscopy (SEM), X-ray photoelectron spectroscopy (XPS), diffuse reflectance spectroscopy (DRS), as well as photoluminescence (PL) measurements. With respect of the degradation of rhodamine B (RhB) under visible light (λ > 420 nm), as compared with undoped Bi_2WO_6, Er^{3+}-doped Bi_2WO_6 exhibited significant enhancement in photocatalytic activity toward the degradation of rhodamine B.

Result and discussion

Characterization of photocatalysts

Fig 1 shows the XRD results of the samples. As can be observed, obvious diffraction peaks were observed for Bi_2WO_6, matching those of Bi_2WO_6 (JCPDS 39-256); peaks were observed at 28.2°, 32.7°, 47.1°, and 55.9°, which correspond to the diffraction peaks of (131), (200), (202), and (133) crystal planes of Bi_2WO_6, respectively. The strongest peak of Bi_2WO_6 was attributed to (131) plane, which is in good agreement with the following high-resolution transmission electron microscopy (HRTEM) analyses. Notably, there were no characteristics of the erbium oxide phase in all samples. The Er^{3+} dopant is hypothesized to not affect the crystal structure of Bi_2WO_6. Nevertheless, because the ionic radius of Bi^{3+} (103 pm) is greater than that of Er^{3+} (89 pm), the lattice parameters of Bi_2WO_6 decrease when Bi^{3+} is substituted by Er^{3+}; therefore, the lattice spacing d decreases.

As shown in the inset in Fig 1, the peaks of Bi_2WO_6:Er^{3+} clearly shifted to higher 2θ angles. Moreover, the cell parameters of undoped Bi_2WO_6 and 1.5% Bi_2WO_6:Er^{3+} were determined from XRD data and were found to be a = 5.459 Å, b = 16.454 Å, c = 5.445 Å for undoped Bi_2WO_6 and a = 5.452 Å, b = 16.439 Å, c = 5.441 Å for Bi_2WO_6:Er^{3+}. The decrease of lattice parameters also corresponds to the result of the shift. The result suggests that Er^{3+} is substituted for fractional Bi^{3+} and is successfully doped into the crystal lattice of Bi_2WO_6.

The morphologies and particle sizes of Bi_2WO_6:Er^{3+} with different contents of Er^{3+} were investigated by SEM, as shown in Fig 2. Fig 2 a–f shows typical SEM images of undoped Bi_2WO_6, 0.5% Bi_2WO_6:Er^{3+}, 1% Bi_2WO_6:Er^{3+}, 1.5% Bi_2WO_6:Er^{3+}, 2% Bi_2WO_6:Er^{3+}, and 3% Bi_2WO_6:Er^{3+}, respectively. From Fig 2a, undoped Bi_2WO_6 exhibited a sheet-like microstructure, with the size of the Bi_2WO_6 nanosheet being approximately 100–200 nm. On the other hand, Bi_2WO_6:Er^{3+} (Fig 2b–f) exhibited a hierarchical flower-like microstructure composed of extensive nanosheets with diameters of approximately 4–5 μm. Clearly, Er^{3+} markedly affected the morphology of Bi_2WO_6. As compared to undoped Bi_2WO_6, these hierarchical flower-like microstructures, composed of extensive nanosheets, exhibited several advantages. On the one hand, these hierarchical flower-like microstructures can absorb more photon energy because of multiple scattering. On the other hand, because of their large surface area, the photogenerated charge carriers can transport electrons to the interface of Bi_2WO_6. Besides, several mesopores serve as transport tracers for improving the transfer rate of small organic molecules. Because of the above-mentioned

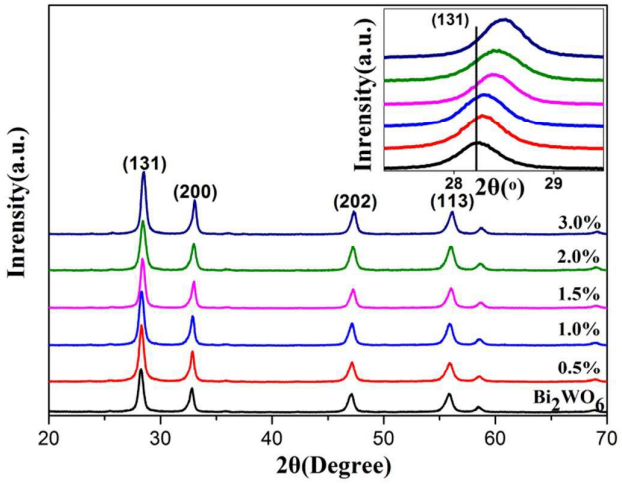

Fig. 1 XRD pattern of Bi_2WO_6:Er^{3+} with Er dopant concentrations (0%, 0.5%, 1%, 1.5%, 2%, 3%). Inset shows the magnification of XRD patterns

reasons, there is enhancement in the photocatalytic activity of Bi_2WO_6:Er^{3+} with hierarchical flower-like microstructures.

Fig. 3 shows the TEM and HRTEM images of 1.5% Bi_2WO_6:Er^{3+}. As shown in Fig 3a, hierarchical flower-like microstructures were clearly observed for 1.5% Bi_2WO_6:Er^{3+}. As shown in Fig 3b, after the dispersion of 1.5% Bi_2WO_6:Er^{3+} in an ultrasonic bath, nanosheets were observed. Fig 3c, d shows HRTEM images of 1.5% Bi_2WO_6:Er^{3+}. As can be observed in the HRTEM images, two sets of lattice fringes were observed with an interplanar spacing of 0.315 nm and 0.273 nm, respectively, which correspond to spacings of (131) and (200) facets of Bi_2WO_6, respectively.

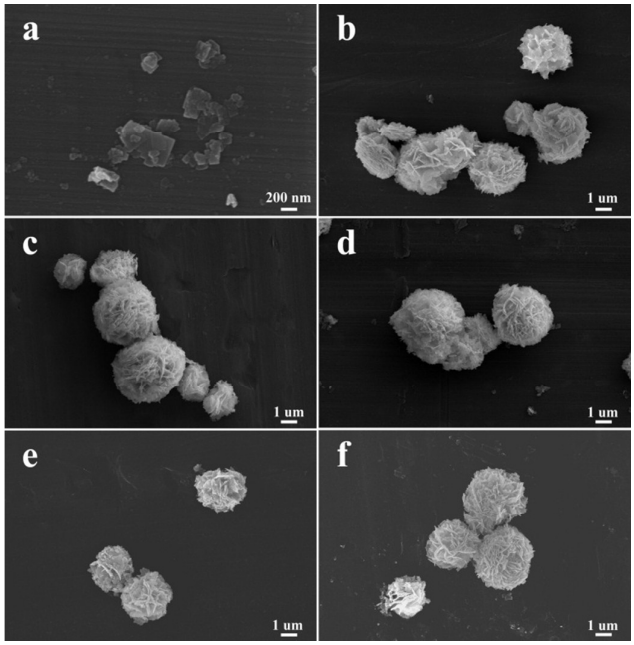

Fig. 2 SEM images of undoped Bi_2WO_6 and Bi_2WO_6:Er^{3+}: (a) undoped Bi_2WO_6, (b) 0.5% Bi_2WO_6:Er^{3+}, (c) 1% Bi_2WO_6:Er^{3+}, (d) 1.5% Bi_2WO_6:Er^{3+}, (e) 2% Bi_2WO_6:Er^{3+}, (f) 3% Bi_2WO_6:Er^{3+}

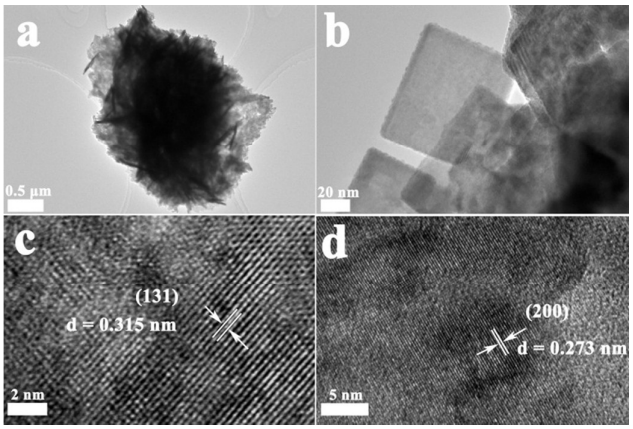

Fig. 3 (a and b) TEM, (c and d) HRTEM images of 1.5% Bi_2WO_6:Er^{3+}

The chemical states and surface compositions of 3% Bi_2WO_6:Er^{3+} (Fig. 4) and 1.5% Bi_2WO_6:Er^{3+} (Fig. S1) were investigated by XPS surface measurements. Fig 4a shows the full scan XPS spectra of 3% Bi_2WO_6:Er^{3+}; Bi, W, O, and Er were detected. Fig 4b–e show high-resolution XPS spectra of four primary elements: Bi 4f, W 4f, O1s, and Er 4d, respectively. Fig 4b shows the XPS spectra of Bi 4f. The major peaks at 159.42 eV and 164.72 eV were assigned to Bi 4f 7/2 and Bi 4f5/2, respectively. As shown in Fig 4c, in the XPS spectra of Bi 4f, peaks were observed at 35.67 eV and 37.82 eV, corresponding to W 4f7/2 and W 4f5/2, respectively. Fig 4d shows the XPS spectrum of O 1s. A peak was observed at 530.34 eV, assigned to the Bi–O bonds in the $(Bi_2O_2)^{2+}$ sheets of the Bi_2WO_6 layered structure. Besides, another peak was observed at 532.15 eV, attributed to the surface hydroxyl groups. As shown in Fig 4e, the binding energy (BE) of Er 4d5/2 increased to 169.8 eV; however, the BE of Er 4d5/2 in erbium oxide has been reported to be 168.0 eV[32], attributed to the Bi–O bonds in the $(Bi_2O_2)^{2+}$ slabs of the Bi_2WO_6 layered structure because of the replacement of Bi by Er. XPS results prove the existence of Er^{3+} in Bi_2WO_6.

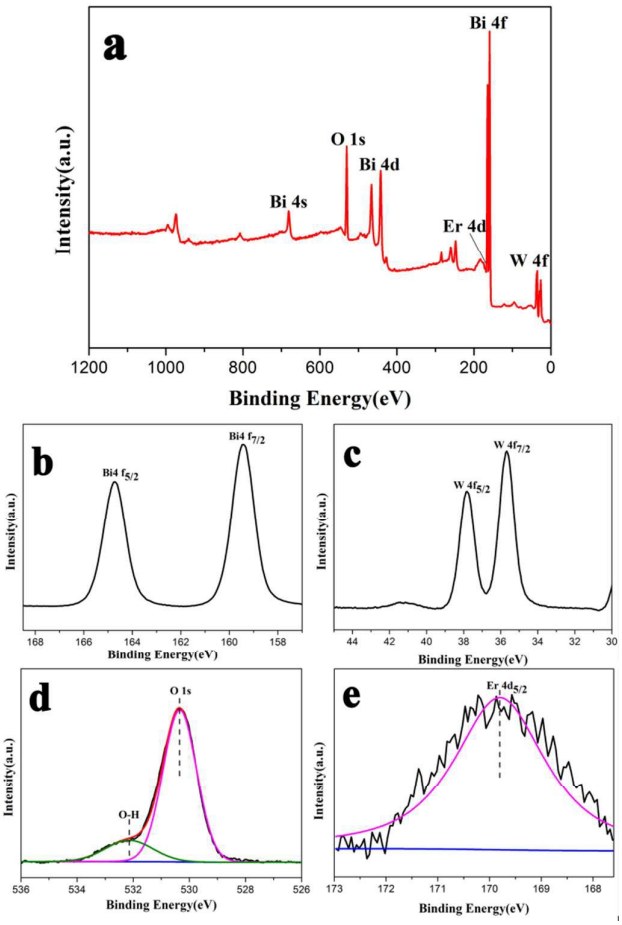

Fig. 4 XPS spectra of the 3.0% Bi_2WO_6:Er^{3+}: (a) survey, (b) Bi 4f, (c) W 4f, (d) O 1s, and (e) Er 4d

Photocatalytic activity

The photocatalytic activities of P25, undoped Bi_2WO_6 and Bi_2WO_6:Er^{3+} were evaluated by the degradation of RhB dye in water under visible light irradiation. Fig. 5a shows the efficiencies of photocatalytic degradation under visible light irradiation. The photolysis of RhB dye was negligible in the absence of the samples, indicating that RhB dye is stable under visible light. Er-doped Bi_2WO_6 exhibited photocatalytic activity significantly better than that exhibited by undoped Bi_2WO_6 and P25. Among these photocatalysts, 1.5% Bi_2WO_6:Er^{3+} exhibited the highest photocatalytic activity, and the photocatalytic degradation of RhB reached 99% within 4 h. As compared to undoped Bi_2WO_6, 1.5% Bi_2WO_6:Er^{3+} exhibited an obviously enhancement in photocatalytic activity. The strongest absorbance of the RhB solution in the visible region shifted from 554 to 500 nm after 4 h of visible irradiation (Fig 5b), reflecting the emergence of N-demethylation and de-ethylation in the photodegradation processes. We research what happens to the total organic content. In the photodegradation process, the major absorption band shifted to 500 nm step by step. Under visible irradiation, deethylation of the fully N,N,N′,N′-tetraethylated rhodamine molecule (i.e., RhB) has the wavelength position of its major absorption band moved toward the blue region, λmax, RhB, 552 nm; N,N,N′-triethylated rhodamine, 539 nm; N,N′-diethylated rhodamine, 522 nm; N-ethylated rhodamine, 510 nm; and rhodamine, 498 nm. Besides, the reaction kinetics of the degradation rate of the RhB solution was quantitatively compared under visible irradiation (λ > 420 nm). The pseudo-first-order model based on the Langmuir–Hinshelwood kinetics model was applied, as shown in the following equations:

$-d[C]/dt = k[C]$.

$-\ln(C/C0) = kt$.

Here, k is the apparent pseudo-first-order rate constant, C_0 is the initial concentration after the adsorption–desorption equilibrium, C is the RhB concentration during the irradiation time. As shown in Fig 5c, from experimental data, the apparent rate constants k of undoped Bi_2WO_6, 0.5% Bi_2WO_6:Er^{3+}, 1.0% Bi_2WO_6:Er^{3+}, 1.5% Bi_2WO_6:Er^{3+}, 2.0% Bi_2WO_6:Er^{3+}, and 3.0% Bi_2WO_6:Er^{3+} were 0.229, 0.565, 0.783, 0.846, 0.458, and 0.413 h^{-1}, respectively. Notably, the photocatalytic activity of 1.5% Bi_2WO_6:Er^{3+} was 3.69 times that of undoped Bi_2WO_6.

Paper

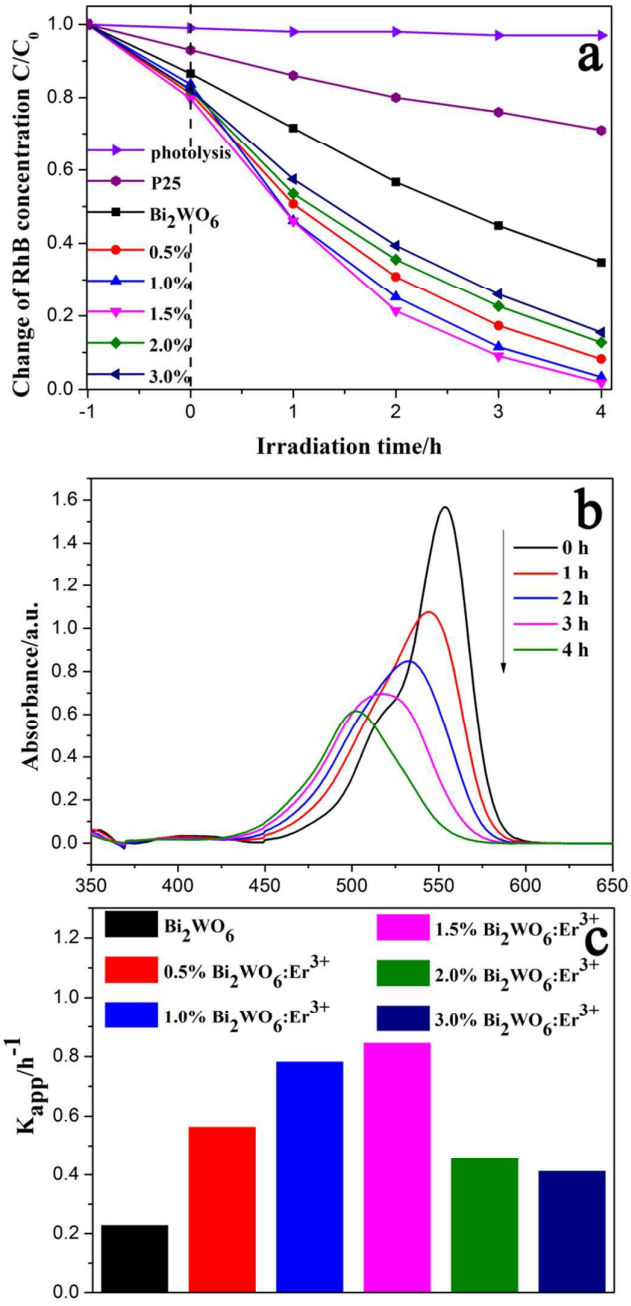

Fig. 5 (a) Photocatalytic degradation curves of RhB over undoped Bi_2WO_6 and Bi_2WO_6:Er^{3+} under visible irradiation (λ > 420 nm) (b) UV–vis spectra of RhB in the presence of 1.5% Bi_2WO_6:Er^{3+} at different irradiation times (visible irradiation) (c) Apparent rate constants for the photodegradation of RhB over undoped Bi_2WO_6 and Bi_2WO_6:Er^{3+} under visible irradiation (λ > 420 nm)

To further investigate the photocatalytic properties of the Bi_2WO_6 and Bi_2WO_6:Er^{3+} catalyst, methyl orange (MO) and methylene blue (MB) dye was also selected to evaluate the photocatalytic activity[33] (Fig. S2). The 1.5% Bi_2WO_6:Er^{3+} catalyst exhibited better photodegraded efficiency for the photocatalytic decomposition of RhB, MO and MB dye under visible-light irradiation. Thus, Er^{3+} doping is an effect way to enhance the photocatalytic activity of Bi_2WO_6.

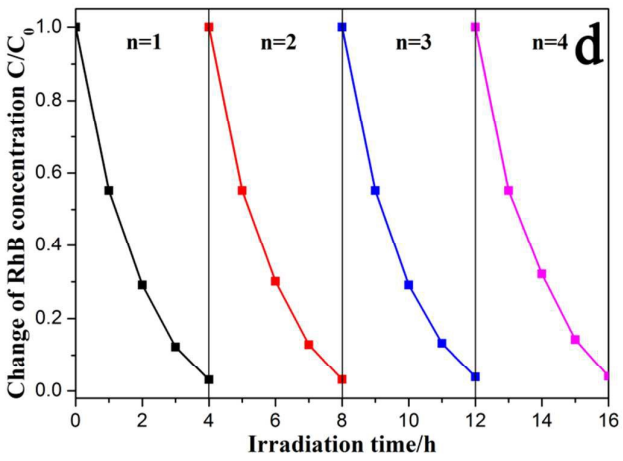

Fig. 6 The stability of the 1.5% Bi_2WO_6:Er^{3+} after 4 cycles for photocatalytic decomposition of RhB under visible irradiation (λ > 420 nm)

To evaluate the stability of the as-prepared 1.5% Bi2WO6:Er^{3+} photocatalysts[33-34], 4 recycling experiments for the photodegradation of RhB were performed (Fig 6). The concentration of RhB during the first run was decreased by 99% after 4 h. After being used 4 times for RhB degradation, the catalyst did not reveal any significant loss of photocatalytic activity.

For elucidating the photocatalytic mechanism in the degradation process of RhB over the Bi_2WO_6:Er^{3+} photocatalyst, trapping experiments were conducted with the aim of detecting active species during the degradation of RhB. For active species trapping experiments, IPA, BQ, and EDTA-2Na were utilized to trap ·OH, superoxide radicals $\cdot O_2^-$, and h^+, respectively. As shown in Fig 7, the degradation of RhB was almost not affected by the addition of 1 mM IPA, indicating that ·OH is dispensable in the photooxidation of RhB. The degradation behavior of RhB obviously decreased with the addition of 1 mM BQ, indicating that $\cdot O_2^-$ plays a significant role in the photooxidation of RhB. Notably, the degradation of RhB almost ceased with the addition of 1 mM EDTA-2Na, indicating that h^+ plays a critical role in the photooxidation of RhB. Thus, trapping experiments of active species demonstrated that $\cdot O_2^-$ and photogenerated h^+ serve as the main active species in the photodegradation of RhB over Bi_2WO_6:Er^{3+} under visible light irradiation.

Bi_2WO_6:Er^{3+} + visble light → Bi_2WO_6:Er^{3+} (e^- + h^+)

h^+ + RhB → degradation

$O_2 + e^- \rightarrow \cdot O_2^-$

$\cdot O_2^-$ + RhB → degradation

In order to further confirm the proposed role of O_2, we do the photocatalytic study under reduced pressure (10 Pa) (Fig. S3). The result is in agreement with the conclusion above.

Mechanism of photocatalytic activity enhancement

Fig 8a shows UV–vis DRS of synthesized samples. As can be observed, the substitution of Bi^{3+} with Er^{3+} resulted in the blue-shift of the absorption edge. For a semiconductor, UV–vis absorption near the band edge follows the equation.

$$Ahv = (\alpha hv - E_g)^{n/2}$$

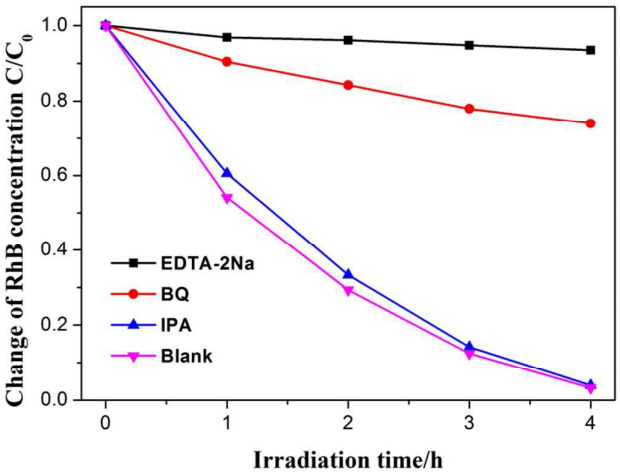

Fig. 7 Photocatalytic degradation of RhB on 1.5% Bi_2WO_6:Er^{3+} alone and with the addition of IPA, BQ, and EDTA-2Na

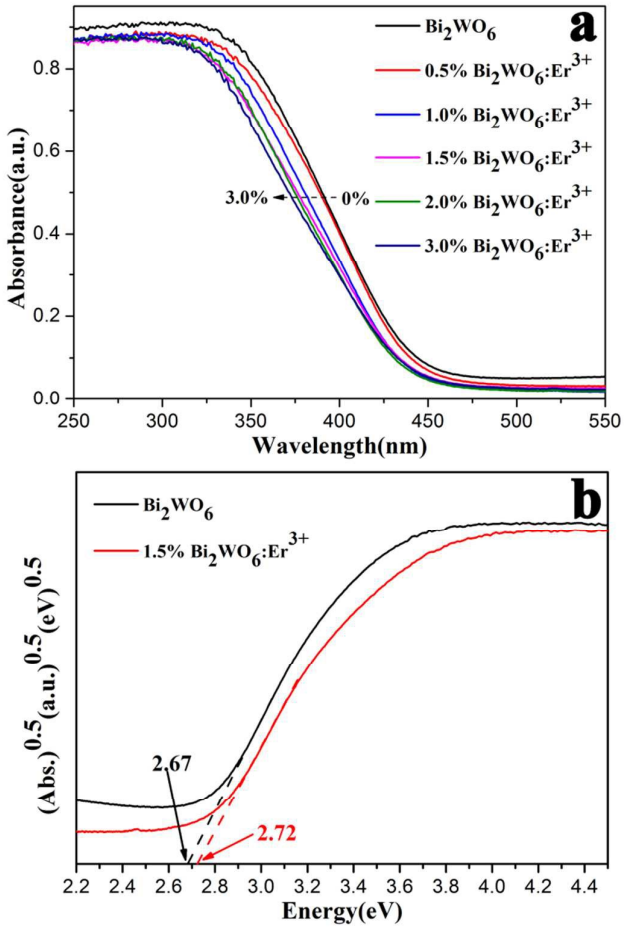

Fig. 8 UV–vis diffuse reflectance spectra (a) and band gaps (b) of undoped Bi_2WO_6 and Bi_2WO_6:Er^{3+}.

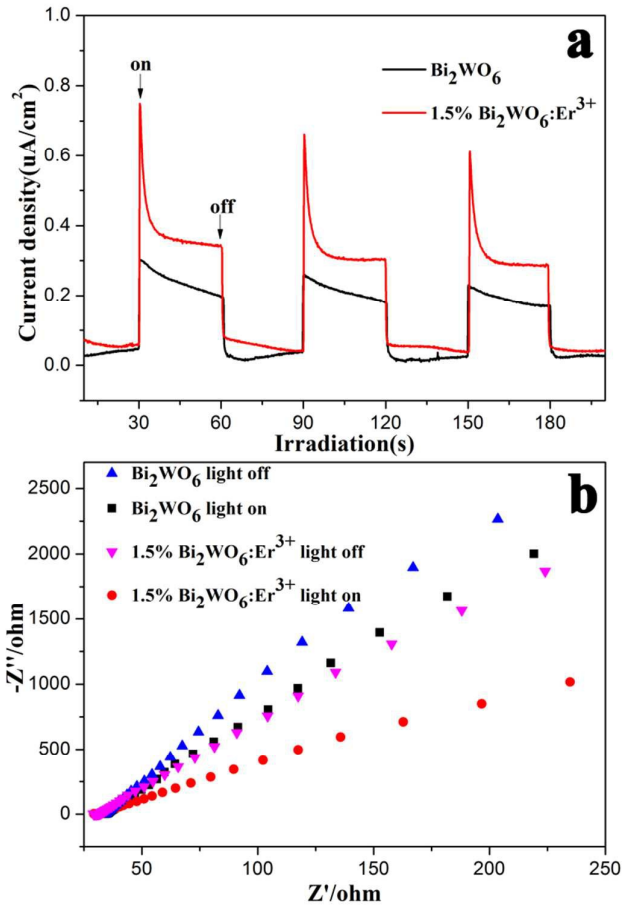

Fig. 9 (a) Photocurrent–time testing curves of undoped Bi_2WO_6 and 1.5% Bi_2WO_6:Er^{3+} under visible light irradiation (λ > 420 nm, [Na_2SO_4] = 0.1 M) (b) Electrochemical impedance spectroscopy (EIS) Nyquist plots of undoped Bi_2WO_6 and 1.5% Bi_2WO_6:Er^{3+} with light on–off cycles under visible light irradiation (λ > 420 nm, [Na_2SO_4] = 0.1 M).

Here, α, v, Eg, and h represent the absorption, light frequency, band gap, and Planck's constant, respectively. The n value is associated with different types of transitions, n = 4 and 1, which correspond to indirect and direct absorption, respectively. Bi_2WO_6 is an indirect band gap-type semiconductor.[35] The band gaps of undoped Bi_2WO_6 and 1.5%Er-Bi_2WO_6 were determined to be 2.67 eV and 2.72 eV, respectively, as shown in Fig 8b.[36] The band gap of 1.5% Bi_2WO_6:Er^{3+} was wider than that of Bi_2WO_6, which is favorable for visible-light-driven photocatalytic activity.[37]

The generation and transfer of the photogenerated charge carriers in the photocatalytic process can be indirectly monitored by the generation of photocurrent.[38] Typically, the higher the photocurrent, the higher the separation efficiency of the photogenerated electron–holes. Fig 9a shows the photocurrent–time testing curves of undoped Bi_2WO_6 and 1.5% Bi_2WO_6:Er^{3+} in the presence or absence of visible light irradiation. As compared to undoped Bi_2WO_6, 1.5% Bi_2WO_6:Er^{3+} exhibited a distinctly enhanced photocurrent response. The results indicate that the photogenerated electron–hole pairs of 1.5% Bi_2WO_6:Er^{3+} could be separated more effectively than those of undoped Bi_2WO_6. Hence, Er^{3+} improves the photoelectrochemical property of Bi_2WO_6.

Paper

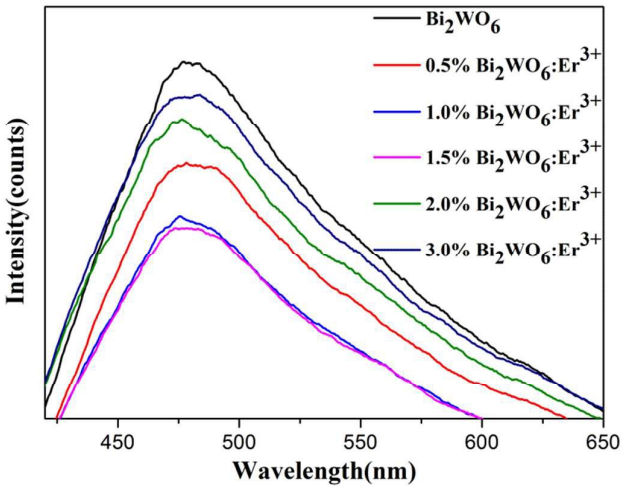

Fig. 10 Photoluminescence spectra of Bi_2WO_6:Er^{3+} (0%, 0.5%, 1%, 1.5%, 2%, and 3%)

Electrochemical impedance spectroscopy (EIS) is an available method for representing the transfer processes of photogenerated electron–holes in the photocatalyst. A small arc radius was observed for the electrode, indicative of low transfer resistance for the interfacial charge carriers. The lower the transfer resistance of the charge carrier, the higher the charge-transfer efficiency. Fig 9b shows the EIS Nyquist plots of undoped Bi_2WO_6 and 1.5% Bi_2WO_6:Er^{3+} in the presence or absence of visible light irradiation. As compared to undoped Bi_2WO_6, 1.5% Bi_2WO_6:Er^{3+} exhibited a smaller charge-transfer resistance.

PL measurements are a useful technique for investigating the recombination rate of the photogenerated electron–hole pairs in a semiconductor, because PL emission mainly results from the recombination of photogenerated electron–hole pairs.[39] In general, a lower PL intensity indicates a lower recombination rate of photogenerated electron–hole pairs, and thus higher photocatalytic activity for semiconductor photocatalysts. Fig 10 shows the PL spectra of the Bi_2WO_6:Er^{3+} photocatalysts at different molar ratios as compared to those of undoped Bi_2WO_6. By contrast, 1.5% Bi_2WO_6:Er^{3+} exhibited the lowest emission intensity, suggesting that it exhibits the highest photocatalytic activity; this result is in agreement with that obtained for the degradation of RhB under visible light.

In the light of the optical property analysis and active species trapping experiments, the possible photocatalytic mechanism of Bi_2WO_6:Er^{3+} under visible light irradiation was clarified in Fig 11. Under visible light irradiation, the photogenerated electrons were excited to the conduction band (CB), and the photogenerated holes were left in the valence band (VB) in the photocatalytic process. The blue-shift of the optical absorption edge occurred after the substitution of Bi^{3+} with Er^{3+}, indicating that some energy levels are formed under the VB. The doping of Er3+ induces a slight modification of band positions. Such small shift, denoted by the band gap value enlargement, clearly affects to the photogenerated charge pairs, causing a better electron hole separation. Besides, under visible light irradiation, the photogenerated electrons were Er^{3+} at the defects sites. Then, the trapped electrons are transferred

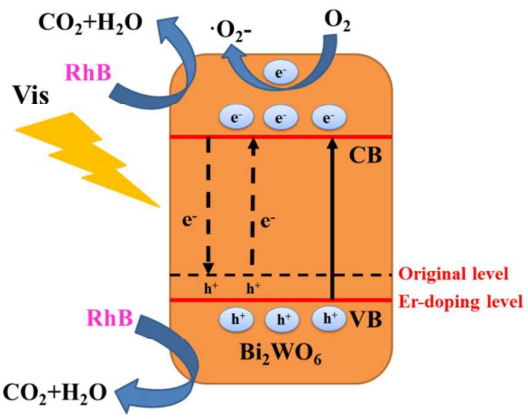

Fig. 11 Schematic of the photocatalytic degradation of RhB on Bi_2WO_6:Er^{3+} under visible light irradiation

to the oxygen molecules adsorbed on the surface of Bi_2WO_6. Those processes can significantly decrease the recombination rate of the photogenerated electron–hole pairs, contributing to the enhanced degradation of RhB by the active hole species. Meanwhile, oxygen molecules adsorbed on the surface of Bi_2WO_6:Er^{3+} can react with the released electrons to generate another active species, $\cdot O_2^-$, for the degradation of RhB. However, those processes can effectively enhance the photocatalytic activity of Bi_2WO_6:Er^{3+}. The possible photocatalytic mechanism was in agreement with the result obtained from the active species trapping experiments. Nevertheless, excess Er^{3+} would cover the active sites or operate as the recombination center on Bi_2WO_6, decreasing the separation efficiency of the photogenerated electron–hole pairs. Hence, the optimum doping concentration of Er^{3+} is 1.5%.

Conclusions

Bi_2WO_6:Er^{3+} with hierarchical flower-like microstructures was successfully synthesized by a one-step hydrothermal method. The result showed that doping with Er^{3+} led to the hierarchical flower-like microstructures of Bi_2WO_6. Under visible light irradiation, 1.5% Bi_2WO_6:Er^{3+} exhibited the highest photocatalytic activity, and the photocatalytic degradation of RhB reached 99% within 4 h. As compared to undoped Bi_2WO_6, 1.5% Bi_2WO_6:Er^{3+} exhibited approximately 3.69 times enhancement in photocatalytic activity as the separation efficiency of the photogenerated electron–hole pairs is enhanced. This study suggests that the use of doping ions into Bi_2WO_6 could be a simple method for the enhancement in photocatalytic activity.

Acknowledgements

This work was financially supported by the National Natural Science Foundation of China (NSFC Grant No.51172216)

Notes and references

1 Fujishima A, Honda K. Photolysis-decomposition of water at the

surface of an irradiated semiconductor[J]. Nature, 1972, 238(5385): 37-38.

2 Hoffmann M R, Martin S T, Choi W, et al. Environmental applications of semiconductor photocatalysis[J]. Chemical reviews, 1995, 95(1): 69-96.

3 Linsebigler A L, Lu G, Yates Jr J T. Photocatalysis on TiO2 surfaces: principles, mechanisms, and selected results[J]. Chemical reviews, 1995, 95(3): 735-758.

4 Wang X, Blechert S, Antonietti M. Polymeric graphitic carbon nitride for heterogeneous photocatalysis[J]. Acs Catalysis, 2012, 2(8): 1596-1606.

5 Cui W, Liu Y, Liu L, et al. Microwave-assisted synthesis of CdS intercalated K 4 Nb 6 O 17 and its photocatalytic activity for hydrogen production[J]. Applied Catalysis A: General, 2012, 417: 111-118.

6 Bellardita M, Addamo M, Di Paola A, et al. Preparation of N-doped TiO 2: characterization and photocatalytic performance under UV and visible light[J]. Physical Chemistry Chemical Physics, 2009, 11(20): 4084-4093.

7 Li D, Bai X, Xu J, et al. Synthesis of CdWO 4 nanorods and investigation of the photocatalytic activity[J]. Physical Chemistry Chemical Physics, 2014, 16(1): 212-218.

8 Yu J C, Yu J, Ho W, et al. Effects of F-doping on the photocatalytic activity and microstructures of nanocrystalline TiO2 powders[J]. Chemistry of materials, 2002, 14(9): 3808-3816.

9 Yang H G, Sun C H, Qiao S Z, et al. Anatase TiO2 single crystals with a large percentage of reactive facets[J]. Nature, 2008, 453(7195): 638-641.

10 Fu H, Pan C, Yao W, et al. Visible-light-induced degradation of rhodamine B by nanosized Bi2WO6[J]. The Journal of physical chemistry B, 2005, 109(47): 22432-22439.

11 Li Y, Liu J, Huang X, et al. Hydrothermal synthesis of Bi2WO6 uniform hierarchical microspheres[J]. Crystal growth & design, 2007, 7(7): 1350-1355.

12 Zhang C, Zhu Y. Synthesis of square Bi2WO6 nanoplates as high-activity visible-light-driven photocatalysts[J]. Chemistry of Materials, 2005, 17(13): 3537-3545.

13 Zhang L, Wang W, Zhou L, et al. Bi2WO6 Nano-and Microstructures: Shape Control and Associated Visible-Light-Driven Photocatalytic Activities[J]. Small, 2007, 3(9): 1618-1625.

14 Zhu S, Xu T, Fu H, et al. Synergetic effect of Bi2WO6 photocatalyst with C60 and enhanced photoactivity under visible irradiation[J]. Environmental science & technology, 2007, 41(17): 6234-6239.

15 Tian N, Zhang Y, Huang H, et al. Influences of Gd substitution on the crystal structure and visible-light-driven photocatalytic performance of Bi2WO6 [J]. The Journal of Physical Chemistry C, 2014, 118(29): 15640-15648.

16 XING G, LI Y, ZHAO Z, et al. Preparation and Photocatalytic Properties of Bismuth Tungsten Oxide Nanomaterials with Different Morphologies [J]. Journal of Synthetic Crystals, 2010, 5: 038.

17 He J, Wang W, Long F, et al. Hydrothermal synthesis of hierarchical rose-like Bi 2 WO 6 microspheres with high photocatalytic activities under visible-light irradiation[J]. Materials Science and Engineering: B, 2012, 177(12): 967-974.

18 GUI M S, WANG P F, YUAN D, et al. Synthesis and visible-light photocatalytic activity of Bi2WO6/gC 3N4 composite photocatalysts[J]. Chinese Journal of Inorganic Chemistry, 2013, 29(10): 2057-2064.

19 Yue D, Chen D, Wang Z, et al. Enhancement of visible photocatalytic performances of a Bi 2 MoO 6–BiOCl nanocomposite with plate-on-plate heterojunction structure[J]. Physical Chemistry Chemical Physics, 2014, 16(47): 26314-26321.

20 Asahi R, Morikawa T, Ohwaki T, et al. Visible-light photocatalysis in nitrogen-doped titanium oxides[J]. science, 2001, 293(5528): 269-271.

21 Gong K, Du F, Xia Z, et al. Nitrogen-doped carbon nanotube arrays with high electrocatalytic activity for oxygen reduction[J]. science, 2009, 323(5915): 760-764.

22 Irie H, Watanabe Y, Hashimoto K. Carbon-doped anatase TiO2 powders as a visible-light sensitive photocatalyst[J]. Chemistry Letters, 2003, 32(8): 772-773.

23 Ohno T, Mitsui T, Matsumura M. Photocatalytic Activity of S-doped TiO2 Photocatalyst under Visible Light[J]. Chemistry Letters, 2003, 32(4): 364-365.

24 Sharma P, Gupta A, Rao K V, et al. Ferromagnetism above room temperature in bulk and transparent thin films of Mn-doped ZnO[J]. Nature materials, 2003, 2(10): 673-677.

25 Amano H, Kito M, Hiramatsu K, et al. P-type conduction in Mg-doped GaN treated with low-energy electron beam irradiation (LEEBI)[J]. Japanese Journal of Applied Physics, 1989, 28(12A): L2112.

26 Guo S, Li X, Wang H, et al. Fe-ions modified mesoporous Bi 2 WO 6 nanosheets with high visible light photocatalytic activity[J]. Journal of colloid and interface science, 2012, 369(1): 373-380.

27 Chen R, Hu C H, Wei S, et al. Synthesis and Activity of Ag-Doped Bi2WO6 Photocatalysts[C] Materials Science Forum. 2013, 743: 560-566.

28 Huang H, Liu K, Chen K, et al. Ce and F comodification on the crystal structure and enhanced photocatalytic activity of Bi2WO6 photocatalyst under visible light irradiation[J]. The Journal of Physical Chemistry C, 2014, 118(26): 14379-14387.

29 Cao R, Huang H, Tian N, et al. Novel Y doped Bi 2 WO 6 photocatalyst: Hydrothermal fabrication, characterization and enhanced visible-light-driven photocatalytic activity for Rhodamine B degradation and photocurrent generation[J]. Materials Characterization, 2015, 101: 166-172.

30 Tian N, Zhang Y, Huang H, et al. Influences of Gd substitution on the crystal structure and visible-light-driven photocatalytic performance of Bi2WO6[J]. The Journal of Physical Chemistry C, 2014, 118(29): 15640-15648.

31 Obregón S, Colón G. Erbium doped TiO 2–Bi 2 WO 6 heterostructure with improved photocatalytic activity under sun-like irradiation[J]. Applied Catalysis B: Environmental, 2013, 140: 299-305.

32 Dzhurinskii B F, Gati D, Sergushin N P, et al. Simple and coordination compounds. An X-ray photoelectron spectroscopic study of certain oxides[J]. Russian Journal of Inorganic Chemistry, 1975, 20: 2307-2314.

33 Guo Y, Zhang G, Liu J, et al. Hierarchically structured α-Fe 2 O 3/Bi 2 WO 6 composite for photocatalytic degradation of organic contaminants under visible light irradiation[J]. RSC Advances, 2013, 3(9): 2963-2970.

34 Shan G, Fu Y, Chu X, et al. Highly active magnetic bismuth tungstate/magnetite composite under visible light irradiation in the

presence of hydrogen peroxide[J]. Journal of colloid and interface science, 2015, 444: 123-131.
35 Fu Y, Chang C, Chen P, et al. Enhanced photocatalytic performance of boron doped Bi 2 WO 6 nanosheets under simulated solar light irradiation[J]. Journal of hazardous materials, 2013, 254: 185-192.
36 Zhang L, Man Y, Zhu Y. Effects of Mo replacement on the structure and visible-light-induced photocatalytic performances of Bi2WO6 photocatalyst[J]. Acs Catalysis, 2011, 1(8): 841-848.
37 Huang H, Qi H, He Y, et al. Enhanced photocatalytic activity of Eu 3+-and Gd 3+-doped BiPO 4[J]. Journal of Materials Research, 2013, 28(21): 2977-2984.
38 Zhang M, Bai X, Liu D, et al. Enhanced catalytic activity of potassium-doped graphitic carbon nitride induced by lower valence position[J]. Applied Catalysis B: Environmental, 2015, 164: 77-81.
39 Cui Y, Jia Q, Li H, et al. Photocatalytic activities of Bi 2 S 3/BiOBr nanocomposites synthesized by a facile hydrothermal process[J]. Applied Surface Science, 2014, 290: 233-239.